Polypeptide-Based "Smart" Micelles for Dual-Drug Delivery: A Combination Study of Experiments and Simulations

Lili Chen, Tao Jiang, Chunhua Cai, Liquan Wang, Jiaping Lin,* and Xuguang Cao*

A dual-drug-loaded micelle is designed and constructed from a mixture of poly(propylene oxide)-*b*-poly(γ-benzyl-L-glutamate)-*b*-poly(ethylene glycol) (PPO-*b*-PBLG-*b*-PEG) triblock terpolymers and two model drugs, doxorubicin (DOX) and naproxen (Nap). In the micelles, the DOX is chemically linked to the PBLG backbones through an acid-cleavable hydrazone bond, whereas the Nap is physically encapsulated in the cores. The drug loading and releasing behaviors of the dual-drug-loaded micelles as well as single drug-loaded micelles (DOX-conjugated or Nap-loaded micelles) are studied. The structures of micelles are characterized by means of microscopies and dynamic light scattering, and further examined by dissipative particle dynamics (DPD) simulations. It is revealed that the micelles possess a core–shell–corona structure in which the PPO/Nap, PBLG/DOX, and PEG aggregate to form the core, shell, and corona, respectively. In vitro studies reveal that the release of DOX and Nap is pH- and thermosensitive. Such drug releasing behaviors are also examined by DPD simulations, and more information regarding the mechanism is obtained. In addition, the bio-related properties such as cellular uptake of the micelles and biocompatibility of the deliveries are evaluated. The results show that the dual-drug-loaded micelles are biocompatible at normal physiological conditions and retain the anti-cancer efficiency.

1. Introduction

In the past decades, polymeric micelles have been comprehensively investigated as drug delivery carriers.[1–7] This is ascribed to their core–shell structure, small size, and the similarity to natural carriers of viruses and serum lipoproteins, which contribute to the bypass of the multidrug resistance effects observed in living cells.[8,9] The hydrophilic shell stabilizes the micelles in the blood circulation, and the hydrophobic core acts as a nano-reservoir for therapeutic agents. The significant challenge for micellar drug delivery is to control the release behavior of drugs in a desired manner, which motivates to construct "smart" micelles from responsive polymers and polymer mixtures.[10,11] Various internal and external stimuli, such as temperature,[12,13] pH,[14–17] redox,[18–21] light,[22,23] and ultrasound[24–27] have been applied to modulate drug release behaviors.

Drug-loaded micelles can be prepared through physical and chemical strategies.[28] The physical method is easy to handle, and drugs are physically confined in the micelle core, however, the uncontrolled release of drugs is the significant shortage. In the chemical strategy, drugs are covalently conjugated to polymer backbones via stimuli-responsive cleavable bonds, and then the conjugates further self-assemble into micelles.[29–33] The polymer–drug conjugate micelles have great advantages in controlling the release of drugs. For example, Kataoka et al. synthesized PEGylated polyaspartate–doxorubicin (DOX) conjugate micelles, in which DOX was attached to polyaspartate backbone via an acid-labile hydrazone bond. It was found that DOX was stable under physiological conditions (pH 7.4), and released under acidic conditions.[14] The chemical conjugated drug-loaded micelles protect drugs from the host defense system in the body, and can accumulate drugs in target tissues, which improves both the delivery effect and therapeutic efficacy of the drugs.[34–38] Among the varieties of micelle-forming polymers, polypeptide-based amphiphilic copolymers have attracted great attentions due to their biocompatibility and the advantages in controlling both the structure and function of the supramolecular aggregates.[39–46]

Combination drug therapy is attractive in clinic applications, which offers advantages such as maximizing therapeutic efficacy, overcoming drug resistance and diminishing side effects.[47–55] Zhang et al. reported targeted nanoparticles for multiple cancer types. They developed nanoparticle–aptamer conjugates to deliver both hydrophobic taxane and hydrophilic nucleic acid intercalating drugs.[51] Both drugs can be released

Dr. L. Chen, T. Jiang, Dr. C. Cai, Dr. L. Wang, Prof. J. Lin, X. Cao
Shanghai Key Laboratory of Advanced Polymeric Materials
Key Laboratory for Ultrafine Materials of Ministry of Education
School of Materials Science and Engineering
East China University of Science and Technology
Shanghai 200237, China
E-mail: caichunhua@ecust.edu.cn; jlin@ecust.edu.cn

DOI: 10.1002/adhm.201300638

from the nanoparticle–aptamer bioconjugates controllably. However, there are limited researches on copolymer micelles of dual-drug delivery systems.[52,53] Discher et al. reported a biodegradable polymersomes to efficiently carry both hydrophobic and hydrophilic anticancer drugs.[54] The polymersomes increase the accumulation of the drugs and cause higher cell death in tumors than free drugs. Due to the limited researches on the dual-drug delivery systems reported so far, developing sophisticated dual-drug delivery systems that can control the release behavior of each drug is eagerly desired.

So far, a number of researches have been reported for the drug delivery systems based on polymeric micelles. However, the releasing mechanisms are still not well understood due to the limitation of current available experimental techniques. To address this challenge, theoretical simulations are ready to tackle these difficulties.[56–58] The simulations such as dissipative particle dynamics (DPD) can provide straightforward microscopic information, and overcome the limitation inherent in experiments. Combining the experiments and simulations is an effective strategy for the investigation of drug release behaviors.

In this paper, we designed a dual-drug-loaded micelle from poly(propylene oxide)-*b*-poly(γ-benzyl-L-glutamate)-*b*-poly(ethylene glycol) (PPO-*b*-PBLG-*b*-PEG) triblock terpolymers, in which hydrophilic PEG blocks form micelle corona, and hydrophobic PBLG and PPO blocks assemble into micelle shell and core, respectively. DOX and naproxen (Nap) were used as model drugs. DOX is chemically conjugated with PBLG block via an acid-labile hydrazone bond, while Nap is physically encapsulated in the micelle core. The pH-sensitive hydrazone linkers and thermo-sensitive PPO segments make the micellar delivery vehicles multi-functional, which is displayed from in vitro drug release behaviors. DPD simulations were used to further verify the structure and the release behavior of the dual-drug-loaded micelle. The simulations allow us to get a deep insight into the mechanism of drug releasing. As far as we know, it is a first example of combination study of experiments and simulations on the drug releasing behaviors of polymeric micelles. In addition, the bio-related research revealed that the micelles can enter the cells, and they can significantly improve the biocompatibility and retention time of drugs.

2. Results and Discussion

This paper consists of three sections: the first section refers to the preparation of DOX/Nap dual-drug-loaded micelles by using PPO-*b*-PBLG-*b*-PEG triblock terpolymers. DOX is chemically linked to shell-forming PBLG blocks (**Scheme 1**), and Nap is physically capsulated in the micelle core. The structure of the micelles was characterized by combination of experiments and DPD simulations. In the second section, the in vitro drug releasing behaviors of the dual-drug-loaded micelles were studied as functions of pH and temperature. And DPD simulations were applied to have a deep insight into the drug release behaviors. In the last section, in order to evaluate the possibility of the applications of the dual drug carrier, we carried out studies on the bio-related properties, including biocompatibility of the deliveries, cellular uptake of the micelles, and retention time of the drugs.

2.1. Structure Studies of Dual-Drug-Loaded Micelles

Dual-drug-loaded micelles were prepared by using a dialysis method. First, PPO-*b*-PBLG-*b*-PEG/DOX conjugates and Nap were separately dissolved with *N*,*N*′-dimethylformamide (DMF) and dimethyl sulfoxide (DMSO) mixture solvent (v/v = 4/1),

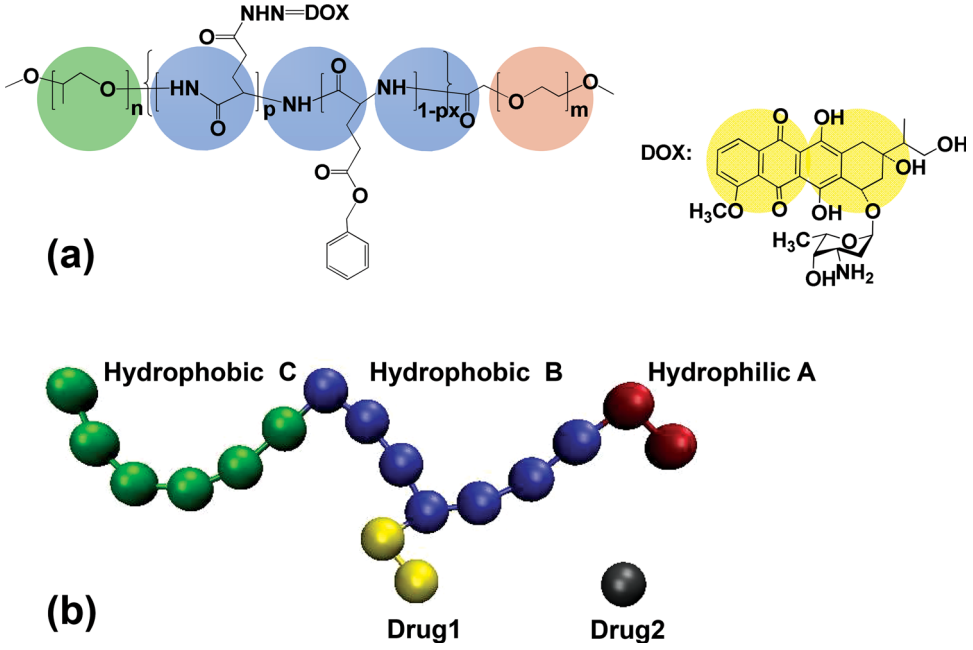

Scheme 1. Mapping between the experimental sample and simulation model: a) structure of DOX-conjugated PPO-*b*-PBLG-*b*-PEG terpolymers; b) DPD model of the dual-drug delivery system.

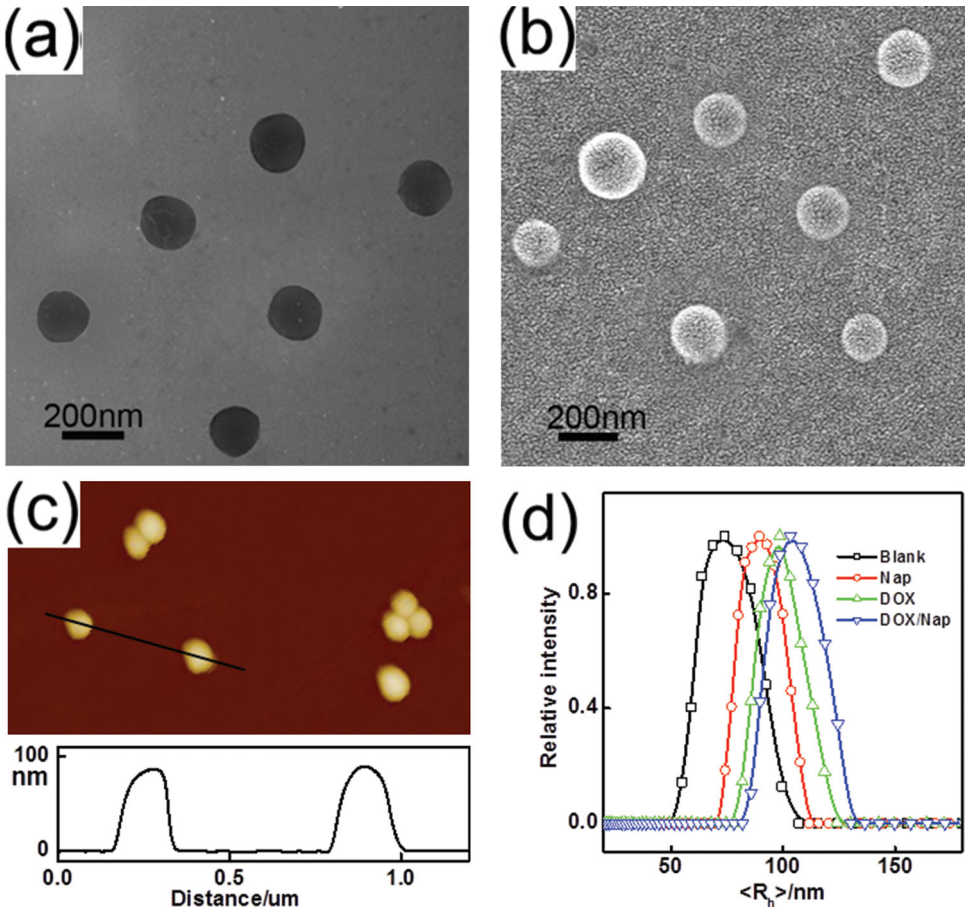

Figure 1. Aggregate morphologies of dual-drug-loaded micelles: a) TEM image; b) SEM image; and c) AFM image. d) The hydrodynamic radius distribution of blank micelles, Nap-loaded micelles, DOX-conjugated micelles, and dual drug-loaded micelles (scattering angle 90°).

and mixed together with volume ratio of 1/1, and then the solution was dialyzed against deionized water. By directly dialyzing the PPO-*b*-PBLG-*b*-PEG triblock terpolymers solution or PPO-*b*-PBLG-*b*-PEG/DOX conjugate solution against deionized water, blank or DOX-conjugated micelle (single drug, chemical method) solutions were prepared. To prepare Nap-loaded micelles (single drug, physical method), Nap solution was mixed with solution of PPO-*b*-PBLG-*b*-PEG triblock terpolymer, and then dialyzed against deionized water.

The morphology of the micelles was observed by transmission electron microscopy (TEM), scanning electron microscopy (SEM), and atomic force microscopy (AFM) testings. Spherical shape was observed for all the micelles. Typically, shown in **Figure 1**a–c are the TEM, SEM, and AFM images for the dual-drug-loaded micelles. The exact aggregate sizes were characterized by dynamic light scattering (DLS) testing, and the results show that the hydrodynamic radii (R_h) are 75, 89, 100, and 105 nm for blank, Nap-loaded, DOX-conjugated, and dual-drug-loaded micelles, respectively. Figure 1d exhibits the hydrodynamic radius distribution ($f(R_h)$) of the micelles (scattering angle 90°). The corresponding polydispersity indices are 0.012, 0.006, 0.008, and 0.006, respectively. Such relative low polydispersity indices imply that those micelles are uniform in size.

Although the microscopy examinations can provide a general insight into the morphology of the aggregates, the detailed structures such as the distributions of drugs and polymer chains are not clear. To gain more information about the micelle structures, a DPD simulation was performed as a complement. A coarse-grained model including **C**-*b*-(**B**-*g*-**Drug1**)-*b*-**A** and **Drug2** (corresponding to PPO-*b*-PBLG-*b*-PEG/DOX conjugate and Nap) was constructed to mimic the dual-drug-loaded micelles self-assembled from mixture of PPO-*b*-PBLG-*b*-PEG/DOX conjugate and Nap (Scheme 1). The mapping between the experimental samples and the DPD models can be referred to the Supporting Information. **Figure 2**a shows the typical simulated structure of the dual-drug-loaded micelles. The triblock terpolymers were found to form micelles with core–shell–corona structure. The core, shell, and corona are occupied by the **C** (PPO), **B** (PBLG), and **A** (PEG) blocks, respectively. The distributions of drugs are clearly shown in Figure 2b, where the density profiles are plotted as a function of the radial direction. As can be seen, the **Drug2** (Nap) is physically encapsulated in the micelle core, while the **Drug1** (DOX) is located in the **B**-block-rich (PBLG-rich) shell region.

2.2. In Vitro Release Behaviors of Dual-Drug-Loaded Micelles

It is of primary importance to reveal the release behaviors of entrapped drugs to guide the design of micellar drug deliveries.

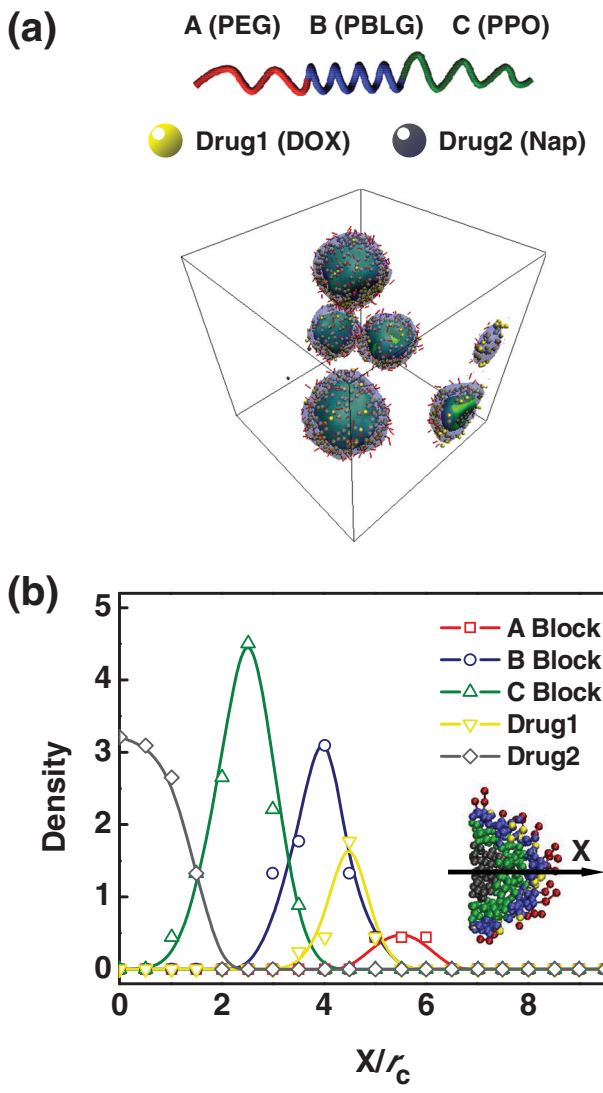

Figure 2. a) Typical simulation snapshots of the drug-loaded system for **ABC** triblock terpolymers in selective solvents. b) 1D density profiles along x-arrow of different segments for terpolymer/drug micelles. The red, blue, green, yellow, and black colors are respectively assigned to **A**, **B**, **C**, **Drug1**, and **Drug2**, while the solvents are omitted for clarity.

For the present system, the drug-releasing behavior can be adjusted by both pH and temperature. The reasons are as follows. 1) Nap is an acidic drug, thus higher pH values can promote faster diffusion of the drug from micelles. 2) The hydrazone linkage can be destroyed at acidic condition, which induces faster release of DOX at lower pH values. In addition, the release of DOX could lead to a loose shell, which favors the diffusion of Nap from micelle core. 3) With increasing temperature, the core-forming PPO blocks are more hydrophobic, and the micelle core shrinks, which can induce faster release of drugs.

The in vitro drug release behaviors of the dual-drug-loaded micelles revealed that DOX and Nap can be controllably released from the micelles. Shown in **Figure 3** is typical release profiles of the drugs at solution condition of pH 5.5 and T = 37 °C. Both the drugs release faster in the initial state, and the

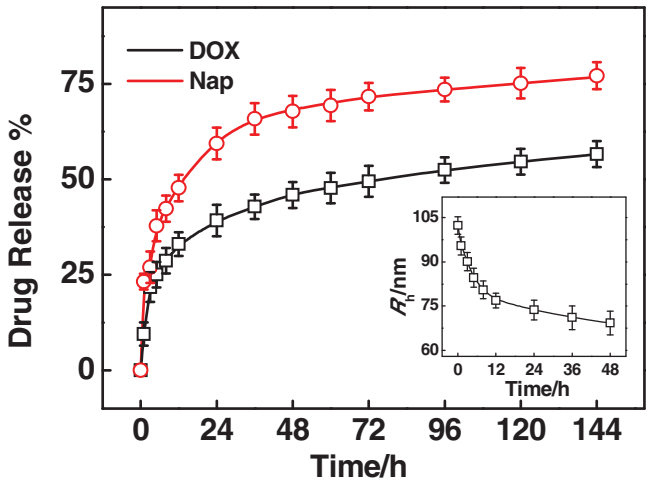

Figure 3. Release profiles of Nap and DOX from dual-drug-loaded micelles. The inset shows the average radius of dual-drug-loaded micelles during drug releasing obtained by DLS. T = 37 °C, pH 5.5.

drugs can release sustainably within 6 d. Upon the release of drugs, the micelles gradually shrink. As shown in the inset, the average R_h value of the micelles, detected by DLS testing, decreases from about 100 nm to 70 nm in 48 h.

We then examined the effect of pH value on the release behavior of dual-drug-loaded micelles (**Figure 4**, T = 37 °C). As shown in Figure 4a, the release of DOX is found to be highly dependent on pH value. At neutral pH condition (pH 7.4), the release rate of DOX is very slow, and the accumulate release amount is about 15% within 6 d. While in acidic solution, the release amount increases to about 55% at pH 5.5 and 70% at pH 4.0. Such a phenomenon is attributed to acid-cleavable nature of the hydrazone linkage between DOX and PBLG backbone.[14] For a comparison, we also examined the release behavior of DOX from single DOX-conjugated micelles. It was found that the release of DOX from DOX-conjugated micelles is also highly dependent on solution pH value. At pH 7.4 (T = 37 °C), about 15% DOX was released within 6 d. When in acidic solution (pH 4.0), the release amount increases to about 60%. This is similar to the situation of the dual-drug-loaded micelles (for details, see Figure S4a, Supporting Information).

Figure 4b shows pH-dependent release behavior of Nap from dual-drug-loaded micelles. It was found that the accumulate release amount slightly increases from about 65% at pH 7.4 to about 80% at pH 4.0 within 6 d. However, as shown in the inset in Figure 4b, the release profile of single Nap-loaded micelles is rather different. The pH effect on the releasing rate is significant, and it decreases from about 80% at pH 7.4 to about 30% at pH 4.0 within 6 d. Such differences may be explained as follows. For single Nap-loaded micelles, the decrease in releasing rate of Nap at acidic condition is due to the lower solubility of Nap.[59] While for dual-drug-loaded micelles, the faster release of DOX at lower pH value gives rise to looser core and shell regions, which induces quick diffusion of Nap from the dual-drug-loaded micelles.

In order to gain more information about the pH-dependent release behaviors, the release behaviors of dual-drug-loaded micelles were further studied by DPD simulations. From the

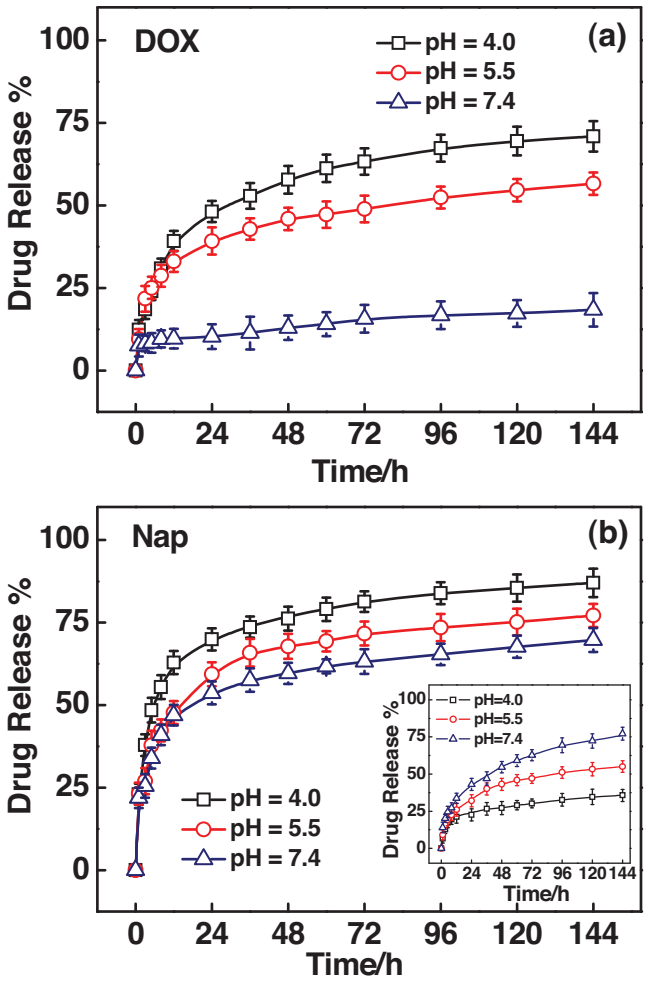

Figure 4. The influence of pH value on the release profiles of a) DOX and b) Nap from dual-drug-loaded micelles. Inset in (b): the release profile of Nap-loaded micelles. $T = 37$ °C.

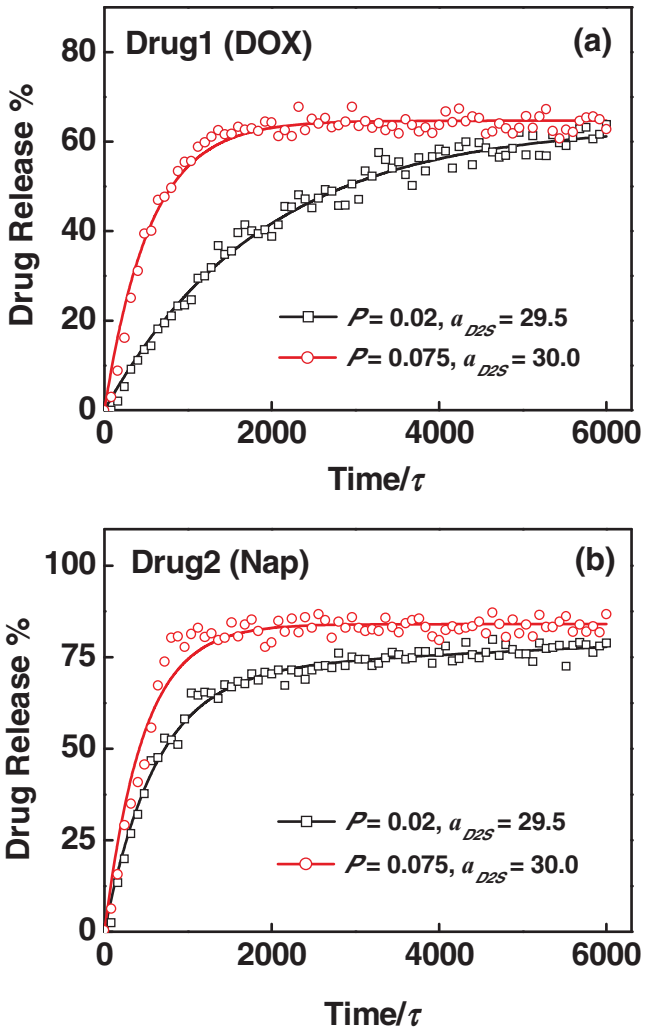

Figure 5. Release profiles of a) **Drug1** and b) **Drug2** from dual-drug-loaded micelles under various pH conditions. The case of $P = 0.02$ and $a_{D2S} = 29.5$ corresponds to a higher pH condition, while the case of $P = 0.075$ and $a_{D2S} = 30.0$ corresponds to a lower pH condition.

above experimental results, we learned that two parameters play important roles in determining the release behaviors of drugs. One is the bond-breaking probability P, which represents the capability of the break of the chemical bonds between the DOX (**Drug1**) and PBLG blocks. The other is the interaction parameter a_{D2S} that controls the solubility of Nap (**Drug2**). As the pH value decreases, the bond-breaking probability P increases but the solubility a_{D2S} of Nap decreases. Accordingly, we chose $P = 0.02$, $a_{D2S} = 29.5$ for high pH value, and $P = 0.075$, $a_{D2S} = 30.0$ for low pH value (the details regarding the setting of parameters are referred to experimental part and Supporting Information). In the simulations, we first seeded the simulations with the equilibrium structures, which are presented in Figure 2. Then, two parameters of P and a_{D2S} were varied to simulate the drug release conditions in the experiments. Finally, we recorded the simulation processes of the drug releases.

Figure 5 shows the simulation results for the drug releases of two different drugs at different pH values. As shown in Figure 5a, the release of **Drug1** depends on the pH values. At a higher pH value ($P = 0.02$ and $a_{D2S} = 29.5$), the release rate of **Drug1** is very slow, and the accumulate release amount is about 50% within time of 4000τ (τ is the time unit). At a lower pH value ($P = 0.075$ and $a_{D2S} = 30.0$), the release amount increases to about 60% within time of 4000τ. The release of **Drug2** is also dependent on the pH values, as shown in Figure 5b. It can be seen that the **Drug2** releases faster at lower pH values. The results presented in both Figure 5a,b imply that both drugs exhibit faster release rates at lower pH value, which is in qualitative accordance with the experimental observations of pH-dependent release behaviors of DOX and Nap in dual-drug-loaded micelles.

In addition to reproducing the release behaviors, the simulations can also give an insight into the releasing processes that the experiments are difficult to follow. **Figure 6** shows the representative simulation snapshots in the releasing process. The parameters were set as $P = 0.075$ and $a_{D2S} = 30.0$, corresponding to a relatively lower pH value. At lower pH values, the Nap has weaker solubility, and the hydrazone bonds between the DOX and PBLG are easier to be broken. As shown

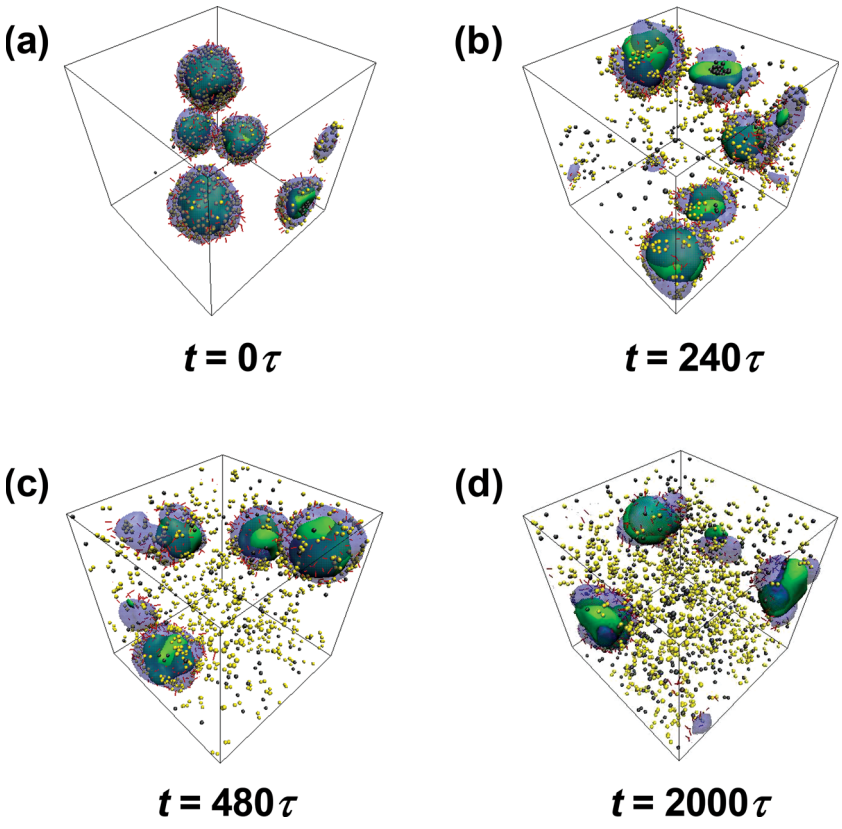

Figure 6. Typical simulation snapshots in the releasing process for **Drug1** and **Drug2** at P = 0.075 and a_{D2S} = 30.0. The simulation times are a) $t = 0\tau$; b) $t = 240\tau$; c) $t = 480\tau$; and d) $t = 2000\tau$.

in Figure 6, the drugs are released gradually with the evolution of simulation time. In the releasing process, the entire micelle structures maintain unchanged to the end of simulation. However, the local structures are varied with the release of the drugs. Such a phenomenon suggests that the structures of micelles are much stable, although the hydrazone bonds are broken and the drugs are released. Since the micelle structures can remain integral in the releasing process, the average radii of dual-drug-loaded micelles were found to decrease. This is in line with the observed phenomena as shown in the inset in Figure 3. These DPD simulation results can well assist the experimental studies. From both experiments and simulations, we can see that the present dual drug carriers exhibit distinctive features. The drugs are loaded within micelles in different ways, that is, chemically bonded and physically encapsulated ways. As a result, the two drugs differ in the releasing fashions, which give rise to a hierarchical releasing behavior in terms of chemical and physical levels.

The release behavior of drugs is also thermosensitive. As shown in **Figure 7**, taking pH 4.0 for example, both DOX and Nap release faster at the higher temperature. The effect of temperature on the releasing rate of Nap is much pronounced. For example, at T = 37 °C, about 90% of Nap was released within 6 d, which is about twice of that at T = 25 °C. While for DOX, with increasing temperature from 25 to 37 °C, the accumulate release amount slightly increases from about 50% to 60%. Due to its thermosensitive nature, increasing temperature makes the PPO blocks more hydrophobic and thus the micelle core shrinks. As a result, the release of physically encapsulated Nap is dramatically accelerated.[5] However, the release of DOX is mainly controlled by the break of hydrazone bond. As a result, the effect of temperature could be less marked. The slight increase in releasing rate of DOX is assigned to the faster diffusion of free DOX from the micelles, which is due to the shrinkage of micelle core at the higher temperature. In addition, the temperature-sensitive effect on drug releasing rate was found to be more pronounced at lower pH values for both the dual-drug-loaded micelles and single drug-loaded micelles. More detailed results can be found in the Supporting Information (Figures S4b, S5, S6).

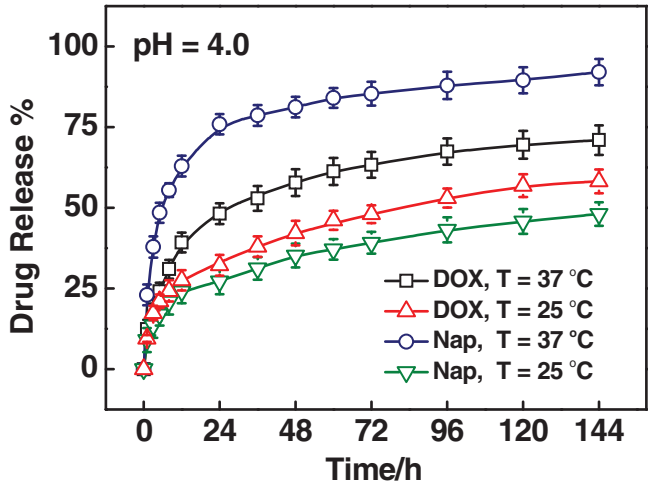

Figure 7. The influence of temperature on the release profiles of DOX and Nap from dual-drug-loaded micelles (pH 4.0).

2.3. Bio-Related Properties of the Drug Deliveries

By taking advantage of physical absorption and chemical bonding, we designed a novel dual-drug-loaded carrier. The release behaviors of each drug are independent and well controlled. Such a system is useful in combined therapy with drugs of different therapeutic effects. In order to evaluate the possibility of the applications of this dual-drug-loaded carrier, we further carried out studies on the bio-related properties, including biocompatibility of the deliveries, cellular uptake of the micelles, and retention time of the drugs.

The biocompatibility was evaluated with in vitro cytotoxicity study of free DOX and drug-loaded micelles against L929 cells by the tetrazolium salt (MTT) assay. The MTT assay is based

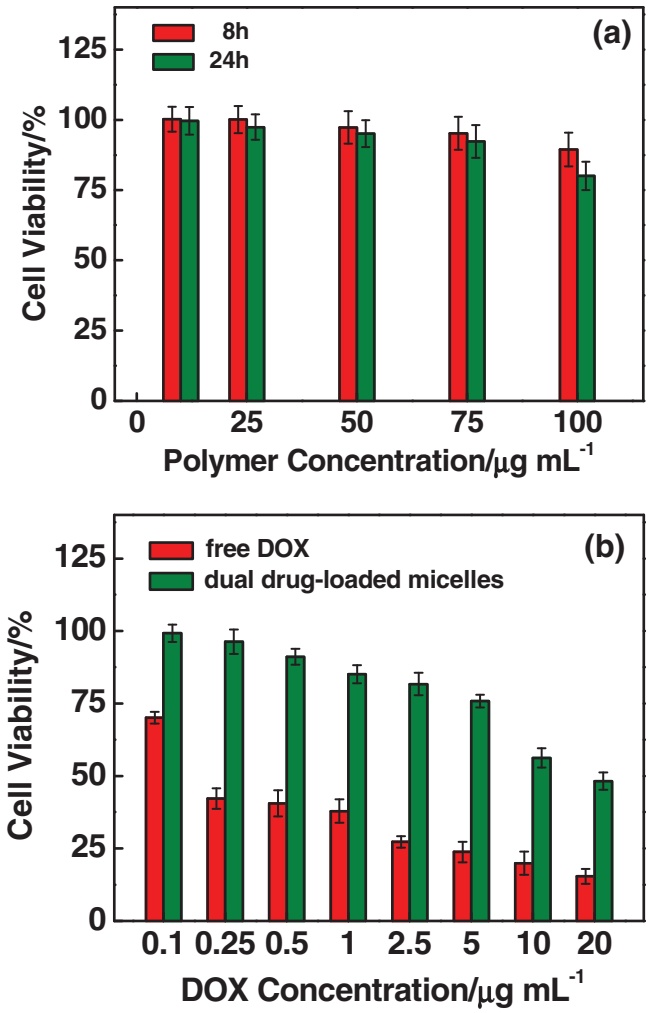

Figure 8. Cytotoxicities of a) blank micelles and b) free DOX and dual-drug-loaded micelles against L929 cells.

on the ability of a mitochondrial dehydrogenation enzyme in viable cells to cleave the tetrazolium rings of the pale yellow MTT and form purple formazan crystals.[49] As shown in **Figure 8**a, there is no obvious cytotoxicity for blank micelles even the concentration reached 100 μg mL^{-1}. In the case of free DOX, the cell viability dramatically decreases by increasing the drug concentration (Figure 8b). However, for dual-drug-loaded micelles, due to the slower release of DOX, much lower cytotoxicity was observed. The improved biocompability of the drug-loaded micelles is also clearly indicated by a great increase of the IC_{50} value (a concentration for 50% cellular growth inhibition) from 0.157 μg mL^{-1} for free DOX to 18.4 μg mL^{-1} for dual-drug-loaded micelles.

The in vitro uptake studies were examined by incubating L929 cells with free DOX and dual-drug-loaded micelles, and the cells were observed with confocal laser scanning microscopy (CLSM). The results revealed that both the free DOX and dual-drug-loaded micelles can be effectively absorbed by L929 cells (**Figure 9**). Figure 9a–d shows the uptake studies of L929 cells treated with free DOX for 2 h. The differential interference contrast (DIC) image shows the cell morphology (Figure 9a), and the cell nuclei was labeled by 4′,6-diamidino-2-phenylindole (DAPI) (blue fluorescence, Figure 9b). Shown in Figure 9c is the red fluorescence emission of free DOX, and Figure 9d shows the merge image of DAPI and DOX fluorescence, which displays that after treated for 2 h, almost all the free DOX molecules were accumulated in the nucleus. For dual-drug-loaded micelles, as shown in Figure 9e–h, DOX are mainly in the cytoplasm of the cells and no significant emission of red fluorescence was observed in the nucleus of the cells (Figure 9g,h). Such observations released important information: 1) free DOX can be quickly transported to the nucleus and bond to the chromosomal DNA; 2) the dual-drug-loaded micelles are stable in the serum-containing medium, no rapid release of DOX accrues; 3) the micelles can be quickly absorbed by L929 cells, but the release of DOX in the cell is slow.

For drug deliveries, relative long circulation time is essential, and it can be characterized by the elimination half-life ($t_{1/2}$) and the area under the plasma concentration–time curve (AUC). **Figure 10** shows the mean plasma concentration–time profiles of drugs after iv administration of dual-drug-loaded micelles as well as free drugs. As compared with free drugs, both the $t_{1/2}$ and AUC values increase for administration of drug-loaded micelles. First, $t_{1/2}$ values dramatically increase from 1.3 to 3.82 h for DOX and from 7.9 to 21.6 h for Nap. Second, the AUC value increases from 6.1 to 21.6 μg h mL^{-1} for DOX, and that for Nap, it increases from 317.8 to 595.8 μg h mL^{-1}. The results revealed that the improved retention of drugs was observed for drug-loaded micelle administration, thus the dosing quantities and frequency can be reduced in clinic treatments.

In the present work, the experimental studies combined with DPD simulations demonstrated a successful design and construction of a dual-drug delivery system. Such a dual-drug-loaded carrier exhibits hierarchical release features, which is controlled in both physical and chemical levels and can be manipulated independently by both pH and temperature. Such delivery systems display some unique advantages for clinlical applications: 1) combined drug delivery: the dual drug delivery system can overcome the poor therapeutic of single drug delivery system; 2) biocompatibility: all the polymer blocks in the system have good biocompatibility and low toxicity; 3) independent drug release: the physical-loaded and chemical-conjugated drugs can be released independently, which meets the clinical requirements; 4) controlled release: in the present dual-drug delivery system, the pH and temperature controlled release behaviors of two drugs allow the carrier selectively release the loaded drugs. We anticipate that this new system could be a promising candidate as dual-drug carrier with controlled release behaviors of each drug in the application of combined therapy.

3. Conclusions

Core–shell–corona micelles self-assembled from PPO-*b*-PBLG-*b*-PEG triblock terpolymers were designed as dual-drug carriers to load hydrophilic Nap and hydrophobic DOX. Nap was physically trapped in the micelle core and DOX was chemically attached to the shell-forming PBLG backbone by acid-cleavable hydrazone bond. The DPD simulations show the structure of

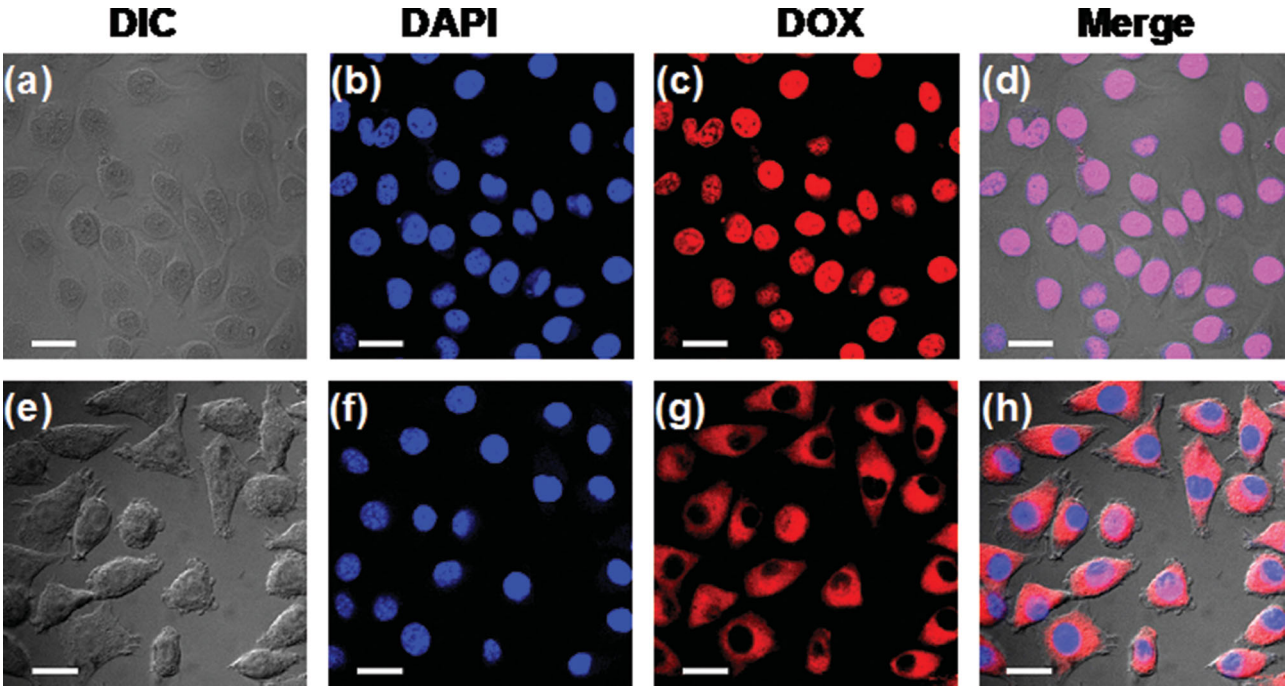

Figure 9. CLSM-images of L929 cells incubated with a–d) free DOX and e–h) dual-drug-loaded micelles. a,e) Differential interference contrast microscopy (DICM) images; b,f) blue fluorescence from DAPI; c,g) red fluorescence from DOX; and d,h) overlap images of blue and red fluorescence. The incubation time is 2 h. Scale bars represent 20 μm.

dual-drug-loaded micelle, i.e., PPO/Nap form the core, PBLG/DOX form the shell, and PEG form the corona. The in vitro release studies revealed that the release rate of DOX from the dual-drug-loaded micelles is faster in acidic solutions. For Nap, when decreasing pH, it releases slightly faster. The pH-sensitive release behaviors are also studied by the DPD simulations, and the detailed releasing process was revealed. Since PPO block is thermosensitive and dehydrated at higher temperatures, the drug release behaviors were also temperature-sensitive, that is, the higher the temperature, the faster the releasing rate of drugs is, especially for the physically encapsulated Nap. The in vivo pharmacokinetics analysis showed that the dual-drug-loaded micelles can enhance therapeutic effects by increasing half-life of drugs. Moreover, the dual-drug-loaded micelles were found to be internalized within the cells and release drugs in the cytoplasm. From these results, it is expected that the functional triblock terpolymers micelles can be utilized to deliver multiple drugs, which tend to act on the same cells and then maximize the therapeutic effect.

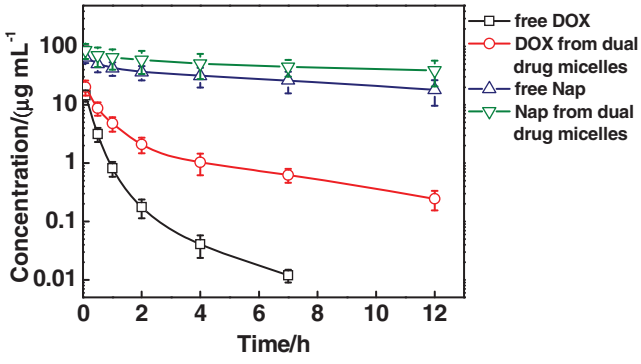

Figure 10. Mean plasma concentration–time profiles of DOX and Nap after intravenous administration ($n = 4$, mean ± SD).

4. Experimental Section

Materials: Doxorubicin hydrochloride (DOX-HCl) was obtained from Zhejiang Hisun Pharmaceutical Co., Ltd. Naproxen was purchased from Shanghai DEMO Chemical Co., Ltd. Dialysis bag (MWCO = 3500) was provided by Serva Electrophoresis GmbH. PPO_{43}-*b*-$PBLG_{23}$-*b*-PEG_{17} triblock terpolymers (the subscripts denote the degree of polymerization of each blocks) and PPO-*b*-PBLG-*b*-PEG/DOX conjugate were synthesized in our lab. The details of the synthesis and characterizations are provided in Supporting Information. All other solvents are of analytical grade and used without further purification.

Preparation of Blank and Drug-Loaded Micelles: Micelles were prepared using a dialysis method. First, PPO-*b*-PBLG-*b*-PEG terpolymer, PPO-*b*-PBLG-*b*-PEG/DOX conjugate or Nap was dissolved with DMF/DMSO mixture solvent (v/v = 4/1) to prepare stock solution (the concentration is 0.6 g L^{-1} for all the solutions). For blank or DOX-conjugated micelles, 5 mL PPO-*b*-PBLG-*b*-PEG polymer or PPO-*b*-PBLG-*b*-PEG/DOX conjugate solution was diluted with equal volume of DMF/DMSO mixture solvent (v/v = 4/1), and then the solution was directly dialyzed against deionized water for 3 d. To prepare Nap-loaded micelle or DOX/Nap dual-drug-loaded micelle solutions, the stock solutions of PPO-*b*-PBLG-*b*-PEG polymer and Nap or PPO-*b*-PBLG-*b*-PEG/DOX conjugates and Nap were mixed with volume ratio of 1/1, and then the mixture solution was dialyzed against deionized water. The aggregate morphologies were examined by TEM (JEOL/JEM-2000EXII) operated at an accelerating voltage of 60 kV. The samples were prepared by dropping 8 μL of micelle solutions on the copper grid coated with carbon film. SEM (S4800, 10 kV) and AFM (XE-100, tapping mode) were also used to characterize the aggregate morphologies. The size

Table 1. Interaction parameters a_{ij} (in DPD units) used in the simulations.

a_{ij}	A (PEG)	B (PBLG)	C (PPO)	Drug1 (DOX)	Drug2 (Nap)	S (Solvent)
A (PEG)	25					
B (PBLG)	80	15				
C (PPO)	80	45	25			
Drug1 (DOX)	80	60	80	25		
Drug2 (Nap)	80	80	45	80	25	
S (Solvent)	15	80	120	45	80	25

of micelles was determined using DLS. DLS was measured by an LLS spectrometer (ALV/CGS-5022F) equipped with an ALV-high QE APD detector and an ALV-5000 digital correlator using a He–Ne laser (the wavelength λ = 632.8 nm) as the light source. The tests were carried out at 20 °C, and solutions were filtered through a 450-nm syringe filter before measurements.

Determination of Drug-Loading Content of the Micelles: To quantify the amount of drug entrapped, 8 mL DMSO was introduced into 2 mL drug-loaded micelle solutions and the mixture was sonicated for 30 min to break up the micelles. The obtained solution was analyzed by an UV–vis spectrometer (UV-2550, SHIMADZU). The characteristic absorbance of DOX at 485 nm and Nap at 331 nm was recorded and compared with standard curve generated from a DMSO/H_2O (v/v = 4/1) mixture with DOX (or Nap) concentrations varying from 0 to 100 μg mL^{-1}. The results show that the drug-loading contents are 20.8 and 18.9 wt% for DOX-conjugated micelles and Nap-loaded micelles. For dual-drug-loaded micelles, the loading contents of DOX and Nap are 18.7 and 10.0 wt%, respectively.

In Vitro Drug Release Study: 2 mL drug-loaded micelle solution was charged in dialysis bag and placed into 5 mL buffer solution with required pH values. Then the samples were laid in a shaking bath at 90 rpm, at 37 °C and 25 °C, respectively. At predetermined time intervals, the buffer solution was replaced by fresh and measured to obtain the amount of released DOX and Nap. The DOX or Nap concentration was determined according to the standard curves of DOX or Nap solution at different pH values.

Cytotoxicity Measurements: The relative cytotoxicity of drug-loaded micelles against L929 cells was estimated by the tetrazolium salt (MTT) assay. L929 cells were seeded into a 96-well plate at a density of 5×10^5 cells per well in DMEM and cultured for 24 h. Then cell culture medium was removed and replaced with 100 μL of a medium containing blank micelles, free DOX, and dual-drug-loaded micelle solution. After another 8 h or 24 h of incubation, the culture medium was removed and the wells were washed twice with PBS solution, and then 100 μL of a 0.5 g L^{-1} MTT solution in PBS was added into each well. After further incubation for 4 h at 37 °C, the medium containing unreacted MTT was removed, and 100 μL of DMSO was added into each well to dissolve the received blue formazan crystals. Finally, the absorbance at 540 nm was measured using a UV–vis spectrometer. The cell viability was calculated as a percentage of absorbance relative to control cells. Each experiment was carried out in triplicate.

Cellular Uptake: The cellular uptake of the micelles was conducted on model cells of L929. The cells were seeded in six-well plates at ≈100 000 cells per well in 2 mL of Dulbecco's modified eagle medium (DMEM) containing 10% fetal bovine serum (FBS), 100 U mL^{-1} penicillin, and 100 μg mL^{-1} streptomycin, and cultured at 37 °C in a humidified atmosphere of 5% CO_2 for 24 h, followed by removing culture medium and adding dual-drug-loaded micelle solution or free DOX solution. The DOX concentration was fixed at 10 μg mL^{-1}. The cells were incubated for 2 h. Then dual-drug-loaded micelle solution or DOX solution was removed, and the cells were rinsed four times with PBS and fixed with 4% formaldehyde for 30 min at room temperature. The cell nuclei were stained with DAPI (blue). Cells were analyzed with CLSM (Olympus FV1000).

Pharmacokinetics: Sprague–Dawlay rats (250–280 g) were allowed food and water ad libitum for at least 4 d before use (the experimental permission was obtained from the Shanghai science and technology committee). The rats were catheterized with sterile silastic cannulae under halothane anesthesia. Then, micelle solutions equivalent to 6 mg kg^{-1} DOX or Nap in saline were administered by intravenous injection. At given time intervals, a series of blood samples (0.5 mL) was collected via arteria cruralis. And, the cannula was rinsed with physiologic saline and with 1 mL diluted heparin to prevent clotting. The contents of DOX and Nap were determined by high-performance liquid chromatography (HPLC, Agilent 110).

Simulation Method and Model: DPD is a mesoscopic simulation technique particularly suitable for complex fluids.[60,61] The dynamics of the elementary units so-called DPD particles is governed by Newton's equations of motion. The detailed description of simulation method can be found in our previous work.[62] To capture the essential features of drug-loaded system for PEG-*b*-PBLG-*b*-PPO triblock terpolymers, we constructed a DPD model of ABC triblock terpolymers grafted by **Drug1**, as typically shown in Scheme 1. **Drug2** (denoted by a single particle) is mixed with the terpolymer bonded by **Drug1**. **Drug1** and **Drug2** represent the DOX and Nap molecules. The triblock terpolymer is denoted as $\mathbf{A}_2\mathbf{B}_7\mathbf{C}_6$, in which the **A**, **B**, and **C** denote the PEG, PBLG, and PPO segments, respectively. The particle number of each block was determined appropriately so that the relative length of the blocks matches the experimental data (see Supporting Information). In the simulations, the concentration of triblock terpolymers grafted by **Drug1** was set as 10.0 vol%, while that of **Drug2** was set as 0.6 vol%. The repulsive parameters between DPD particles are listed in **Table 1**. We carried out the simulations over a long time to equilibrate the drug-loaded micelle structures.

After enough equilibration, drug release tests were performed for another long time. Taking the stable drug-loaded system as an initial state, the solvent environment was varied, which may give rise to the change in drug solubility or breaking of chemical bonds. As a result, the drugs could be released from the hybrid micelles self-assembled from copolymer/drug mixtures. The **Drug1** can be released through the breaking of the bonds between **Drug1** and **B** block. Based on the acid-cleavable nature of the hydrazone linkage between PBLG and DOX, the bonds between the copolymers and **Drug1** were permanently broken with a probability *P* by randomly selecting the bonds every 1000 steps. We applied the reaction dynamics to simulate the breaking process of the hydrazone bonds (see Supporting Information). It can be found at a fixed time interval, *P* is independent of the reaction time and drug concentration, but only depends on the velocity constant *k*. *k* is associated with the pH, and at a lower pH *k* is larger (*P* is also larger). Therefore, the increase in *P* can correspond to the decrease of pH.

Supporting Information

Supporting Information is available from the Wiley Online Library or from the author.

Acknowledgements

This work was supported by National Natural Science Foundation of China (21234002 and 51303055), Key Grant Project of Ministry

of Education (313020), National Basic Research Program of China (No. 2012CB933600) and Research Fund for the Doctoral Program of Higher Education of China (20120074120001). Support from projects of Shanghai municipality (10GG15 and 12ZR1442500) and Fundamental Research Funds for the Central Universities (WD1214008) are also appreciated.

Received: November 15, 2013
Revised: February 21, 2014
Published online: March 20, 2014

[1] Z. Ge, S. Liu, *Chem. Soc. Rev.* **2013**, *42*, 7289
[2] J.-F. Gohy, *Adv. Polym. Sci.* **2005**, *190*, 65.
[3] K. Kataoka, A. Harada, Y. Nagasaki, *Adv. Drug Delivery Rev.* **2001**, *47*, 113.
[4] B. Wang, R. Ma, G. Liu, Y. Li, X. Liu, Y. An, L. Shi, *Langmuir* **2009**, *25*, 12522.
[5] J. Lin, J. Zhu, T. Chen, S. Lin, C. Cai, L. Zhang, Y. Zhuang, X.-S. Wang, *Biomaterials* **2009**, *30*, 108.
[6] G. Cai, H. Zhang, P. Liu, L. Wang, H. Jiang, *Acta Biomater.* **2011**, *7*, 3729.
[7] W. Lin, D. Kim, *Langmuir* **2011**, *27*, 12090.
[8] X. Liu, R. Ma, J. Shen, Y. Xu, Y. An, L. Shi, *Biomacromolecules* **2012**, *13*, 1307.
[9] S. H. Kim, J. H. Jeong, C. O. Joe, T. G. Park, *J. Controlled Release* **2005**, *103*, 625.
[10] C.-K. Huang, C.-L. Lo, H.-H. Chen, G.-H. Hsiue, *Adv. Funct. Mater.* **2007**, *17*, 2291.
[11] Y. Chen, X.-H. Pang, C.-M. Dong, *Adv. Funct. Mater.* **2010**, *20*, 579.
[12] H. Xu, F. Meng, Z. Zhong, *J. Mater. Chem.* **2009**, *19*, 4183.
[13] Y. Li, B. S. Lokitz, C. L. McCormick, *Angew. Chem. Int. Ed.* **2006**, *45*, 5792.
[14] Y. Bae, S. Fukushima, A. Harada, K. Kataoka, *Angew. Chem. Int. Ed.* **2003**, *42*, 4640.
[15] V. W.-W. Yam, Y. Hu, K. H.-Y. Chan, C. Y.-S. Chung, *Chem. Commun.* **2009**, 6216.
[16] L. Zhao, L. Zhu, F. Liu, C. Liu, Shan-Dan, Q. Wang, C. Zhang, J. Li, J. Liu, X. Qu, Z. Yang, *Int. J. Pharm.* **2011**, *410*, 83.
[17] R. Liu, D. Li, B. He, X. Xu, M. Sheng, Y. Lai, G. Wang, Z. Gu, *J. Controlled Release* **2011**, *152*, 49.
[18] J.-H. Ryu, R. Roy, J. Ventura, S. Thayumanavan, *Langmuir* **2010**, *26*, 7086.
[19] L.-Y. Tang, Y.-C. Wang, Y. Li, J.-Z. Du, J. Wang, *Bioconjugate Chem.* **2009**, *20*, 1095.
[20] Y.-C. Wang, F. Wang, T.-M. Sun, J. Wang, *Bioconjugate Chem.* **2011**, *22*, 1939.
[21] H. Wen, C. Dong, H. Dong, A. Shen, W. Xia, X. Cai, Y. Song, X. Li, Y. Li, D. Shi, *Small* **2012**, *8*, 760.
[22] J. Jiang, X. Tong, Y. Zhao, *J. Am. Chem. Soc.* **2005**, *127*, 8290.
[23] J. Jiang, X. Tong, D. Morris, Y. Zhao, *Macromolecules* **2006**, *39*, 4633.
[24] G. A. Husseini, G. D. Myrup, W. G. Pitt, D. A. Christensen, N. Y. Rapoport, *J. Controlled Release* **2000**, *69*, 43.
[25] N. Rapoport, *Int. J. Pharm.* **2004**, *277*, 155.
[26] R. Tong, H. Xia, X. Li, *J. Mater. Chem. B* **2013**, *1*, 886.
[27] Y. Li, R. Tong, H. Xia, H. Zhang, J. Xuan, *Chem. Commun.* **2010**, *46*, 7739.
[28] J. M. Morachis, E. A. Mahmoud, A. Almutairi, *Pharmacol. Rev.* **2012**, *64*, 505.
[29] Y.-F. Huang, D. Shangguan, H. Liu, J. A. Philips, X. Zhang, Y. Chen, W. Tan, *ChemBioChem* **2009**, *10*, 862.
[30] S. Modi, J. Prakash, A. J. Domb, N. Kumar, *Curr. Pharm. Design* **2006**, *12*, 4785.
[31] H. S. Yoo, E. A. Lee, T. G. Park, *J. Controlled Release* **2002**, *82*, 17.
[32] E. R. Gillies, A. P. Goodwin, J. M. J. Fréchet, *Bioconjugate Chem.* **2004**, *15*, 1254.
[33] N. Murthy, Y. X. Thng, S. Schuck, M. C. Xu, J. M. J. Fréchet, *J. Am. Chem. Soc.* **2002**, *124*, 12398.
[34] Y. Lee, Y. Park, H. Mok, T. G. Park, *Bioconjugate Chem.* **2008**, *19*, 525.
[35] E. R. Gillies, J. M. J. Fréchet, *Bioconjugate Chem.* **2005**, *16*, 361.
[36] P. Chytil, T. Etrych, Č. Koňák, M. Šírová, T. Mrkvan, B. Říhová, K. Ulbrich, *J. Controlled Release* **2006**, *115*, 26.
[37] S. J. Guillaudeu, M. E. Fox, Y. M. Haidar, E. E. Dy, F. C. Szoka, J. M. J. Fréchet, *Bioconjugate Chem.* **2008**, *19*, 461.
[38] M. Prabaharan, J. J. Grailer, S. Pilla, D. A. Steeber, S. Gong, *Biomaterials* **2009**, *30*, 5757.
[39] C. Cai, Y. Li, J. Lin, L. Wang, S. Lin, X.-S. Wang, T. Jiang, *Angew. Chem. Int. Ed.* **2013**, *52*, 7732.
[40] L. Wu, Y. Zou, C. Deng, R. Cheng, F. Meng, Z. Zhong, *Biomaterials* **2013**, *34*, 5262.
[41] C. Cai, J. Lin, Z. Zhuang, W. Zhu, *Adv. Polym. Sci.* **2013**, *259*, 159.
[42] J. G. Ray, A. J. Johnson, D. A. Savin, *J. Polym. Sci., Part B: Polym. Phys.* **2013**, *51*, 508.
[43] C. Cai, L. Wang, J. Lin, *Chem. Commun.* **2011**, *47*, 11189.
[44] C. He, X. Zhuang, Z. Tang, H. Tian, X. Chen, *Adv. Healthcare Mater.* **2012**, *1*, 48.
[45] A. Carlsen, S. Lecommandoux, *Curr. Opin. Colloid Interface Sci.* **2009**, *14*, 329.
[46] H. Iatrou, H. Frielinghaus, S. Hanski, N. Ferderigos, J. Ruokolainen, O. Ikkala, D. Richter, J. Mays, N. Hadjichristidis, *Biomacromolecules* **2007**, *8*, 2173
[47] C. Walsh, *Nature* **2000**, *406*, 775.
[48] S. Mitragotri, *Pharm. Res.* **2000**, *17*, 1354.
[49] Y. H. Bae, L. Y. Qiu, *Biomaterials* **2007**, *28*, 4132.
[50] L. Wei, C. Cai, J. Lin, T. Chen, *Biomaterials* **2009**, *30*, 2606.
[51] S. Aryal, C.-M. J. Hu, L. Zhang, *Small* **2010**, *6*, 1442.
[52] L. Zhang, A. F. Radovic-Moreno, F. Alexis, F. X. Gu, P. A. Basto, V. Bagalkot, S. Jon, R. S. Langer, O. C. Farokhzad, *ChemMedChem* **2007**, *2*, 1268.
[53] F. Dilnawaz, A. Singh, C. Mohanty, S. K. Sahoo, *Biomaterials* **2010**, *31*, 3694.
[54] U. Manna, S. Patil, *Langmuir* **2009**, *15*, 10515.
[55] F. Ahmed, R. I. Pakunlu, A. Brannan, F. Bates, T. Minko, D. E. Discher, *J. Controlled Release* **2006**, *116*, 150.
[56] J. Siepmann, A. Göpferich, *Adv. Drug Delivery Rev.* **2001**, *48*, 229.
[57] C.-C. Lin, A. T. Metters, *Adv. Drug Delivery Rev.* **2006**, *58*, 1379.
[58] W. Kong, B. Li, Q. Jin, D. Ding, A.-C. Shi, *J. Am. Chem. Soc.* **2009**, *131*, 8503.
[59] J. Lin, S. Zhang, T. Chen, S. Lin, H. Jin, *Int. J. Pharm.* **2007**, *336*, 49.
[60] P. J. Hoogerbrugge, J. M. V. A. Koelman, *Europhys. Lett.* **1992**, *19*, 155.
[61] J. M. V. A. Koelman, P. J. Hoogerbrugge, *Europhys. Lett.* **1993**, *21*, 363.
[62] T. Jiang, L. Wang, S. Lin, J. Lin, Y. Li, *Langmuir* **2011**, *27*, 6440.

